Chemical Engineering Journal 146 (2009) 338–344

Contents lists available at ScienceDirect

Chemical Engineering Journal

journal homepage: www.elsevier.com/locate/cej

Separation of ternary hydrocarbon mixtures on Y zeolite membranes

Adolfo M. Avila, Ulises Sedran*

Instituto de Investigaciones en Catálisis y Petroquímica, INCAPE (FIQ, UNL-CONICET), Santiago del Estero 2654, 3000 Santa Fe, Argentina

ARTICLE INFO

Article history:
Received 11 December 2007
Received in revised form 13 June 2008
Accepted 17 June 2008

Keywords:
Zeolite membrane
Transient permeation
Multicomponent transport

ABSTRACT

The permeation of a mixture of *n*-hexane, *n*-decane and toluene through a 40 μm Y zeolite tubular membrane on a support with negligible resistance to the mass transfer at 250 °C was modelled based on the Maxwell–Stefan formulation and the ideal adsorbed solution theory (IAST). Individual adsorption parameters were obtained with a batch fluidized bed reactor and diffusion parameters were taken from the literature. The model allowed to predict the transient fluxes and surface coverages through the membrane, showing that the responses of the components diffusing faster (*n*-hexane and *n*-decane) overshoot their steady-state values. The permeance predictions (10^{-8} mol/s m^2 Pa) ranged from 1.2 to 20 for *n*-decane, from 0.4 to 4.2 for *n*-hexane and from 0.8 to 4.0 for toluene, according to the feed pressure and composition. The permeance selectivities, defined with *n*-hexane as the reference, ranged between 3 and 6 for *n*-decane, and between 1 and 1.8 for toluene. It was also possible to define the association between hydrocarbon coverage profiles in the membrane and the corresponding resulting fluxes.

1. Introduction

During the past years there has been an extraordinary increase in research about membranes for the separation and purification of multicomponent gas mixtures. Many of the challenges in the area, related to diffusion–adsorption phenomena, are focused on miniaturized devices for microreactors and microseparators [1–3], various gas sensors [4] and "Lab on a Chip" technologies [5], where zeolite films have promising prospects [6].

One of the common issues in the characterization of zeolite membranes that are applied to the separation of hydrocarbon mixtures is the assessment of individual fluxes and further estimation of ideal selectivities. This means that the species are assumed to diffuse independently across the membrane. However, this kind of characterization renders incomplete information, since the fluxes in a mixture of species can be quite different from those of the single components, and it has been shown that the transport selectivities resulting from the permeation of the various hydrocarbons composing a mixture across zeolite membranes cannot be predicted from the permeances of the single components [7]. Among many factors, competitive adsorption, pore mouth blocking and/or single file diffusion, added to the difficulty of experimentation with mixtures may contribute to define complex interactions. Moreover, there is a substantial increase in the complexity of simulations when a large number of components is involved [8].

The ability to predict the transient behavior of multicomponent gas mixtures is useful for the analysis of the dynamic responses in the design of microreactors, gas sensors or other devices. The macroscopic description of mixture transport processes in novel zeolite materials requires the knowledge of diffusion and adsorption parameters of the species involved. It is commonly accepted that the generalized Maxwell–Stefan formulation offers the most convenient and nearest quantitative prediction of multicomponent diffusion through zeolite membranes [9]. The strength of this model lies on the fact that it is based on the intracrystalline diffusivities of the pure components and the mixture adsorption isotherms. In that sense, the ideal adsorbed solution theory (IAST) [10] is a model adequate for representing the adsorption of mixtures of species with different saturation capacities [11]. Consequently, this type of separation processes can be analyzed by means of the prediction of the corresponding fluxes, surface coverages, permeances and selectivities starting from the individual diffusion and adsorption parameters.

Most of the works about the transient adsorption response of mixtures in zeolite adsorbents considered binary systems and extended Langmuir isotherms [12,13], and studies on the dynamic transport of ternary mixtures, particularly those with mixture isotherms described by the IAST model [14,15], are rather scarce [16].

FAU-type zeolites have large pores defined by 12 member-rings and faujasite structure [17]. Consequently, in comparison with other small or medium pore zeolites, such zeolites can accommodate larger molecules within its structure. The composition of Y zeolite implies that the structural Si/Al ratio is larger than 2. These

* Corresponding author. Tel.: +54 342 452 8062; fax: +51 342 453 1068.
E-mail address: usedran@fiqus.unl.edu.ar (U. Sedran).

1385-8947/$ – see front matter © 2008 Elsevier B.V. All rights reserved.
doi:10.1016/j.cej.2008.06.011

Nomenclature

b	Langmuir adsorption constant (kPa^{-1})
$\mathbf{B}$	sorbate–sorbate interaction matrix (s/m^2)
D_0	zero coverage diffusivity (m^2/s)
$D_{0,i,j}$	diffusion exchange coefficients between components i and j
IAST	IAST isotherm
K	Henry adsorption constant (dimensionless)
N	molar flow ($mol/m^2\ s$)
$\underline{N}$	multicomponent molar flow vector ($mol/m^2\ s$)
P	pressure or partial pressure (kPa)
q	local concentration of species adsorbed on the catalyst (mol/kg)
$\mathbf{q}_s$	diagonal matrix of saturation adsorption capacities (mol/kg)
r	radial length dimension (m)
R	membrane radius, external (m)
S	adsorption or permeance selectivity
t	time (s)
y	mole fraction in the gas phase

Subscripts

C6	n-hexane
C10	n-decane
feed	feed side
i	components i
i,j	cross-term between components i and j
perm	permeate side
s	adsorption capacity at saturation
TOL	toluene
z	zeolite

Superscript

eq	equilibrium

Greek letters

$\mathbf{\Gamma}$	matrix of thermodynamic correction factors
δ	membrane thickness (m)
θ	fractional coverage
$\nabla\theta$	multicomponent fractional coverage gradient vector
$\prod$	permeance ($mol/s\ m^2\ Pa$)
ρ	density (kg/m^3)

materials are versatile in the sense that the permeation properties of different chemical species could be modified by zeolite ion exchange or dealumination [18], and thus tailor-made membranes based on faujasite-type crystals can be obtained for specific applications. Several research groups have reported the synthesis of NaY or NaX (Si/Al ratio about 1.0–1.5) membranes on porous alumina supports [19–21].

It is the objective of this work to examine the modelling and the simulation results for the separation of a mixture of n-hexane, n-decane and toluene through a 40 μm thickness Y zeolite tubular membrane for various system pressures and compositions at 250 °C.

2. System modelling

A schematic representation of the tubular zeolite membrane considered can be observed in Fig. 1. The feed and permeate zones are located outside and inside the infinite hollow cylindrical membrane, respectively. The 40 μm defect-free zeolite membrane is supported on a material with negligible resistance to the mass transfer, and a large volumetric flow of a sweeping gas is circulated in the permeate duct, thus leading to negligible partial pressures of the hydrocarbons in the permeate side. Adsorption equilibria are assumed to be achieved on the feed side of the membrane. The ternary adsorption equilibrium in the membrane is calculated according to the ideal adsorbed solution theory [10], considering Langmuir-type adsorption for the single components. Chemical reactions do not proceed under the conditions studied.

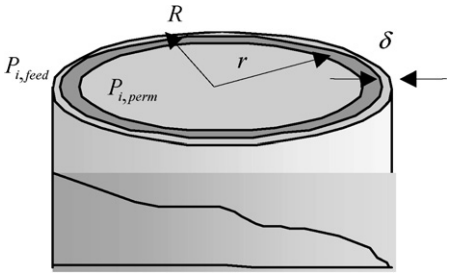

Fig. 1. Supported zeolite tubular membrane.

Then, the mass balance for a given hydrocarbon inside the membrane is

$$\rho_z \frac{\partial q_i(r,t)}{\partial t} = -\frac{1}{r}\frac{\partial}{\partial r}(rN_i) \tag{1}$$

where the diffusion flux through the zeolite is considered configurational and described by the Maxwell–Stefan model [3]:

$$\underline{N} = -\rho_z \mathbf{q}_s \mathbf{B}^{-1} \mathbf{\Gamma} \nabla\theta \tag{2}$$

where

$$\Gamma_{ij} \equiv \frac{\theta_i}{P_i}\frac{\partial P_i}{\partial \theta_j} \tag{3}$$

$$B_{ii} = \sum_{\substack{j=1 \\ j\neq i}}^{n} \frac{\theta_j}{D_{0,i,j}} + \frac{1}{D_{0,i}}, \qquad B_{ij} = -\frac{\theta_i}{D_{0,i,j}}; \quad i \neq j \tag{4}$$

$$q_{s,ii} = q_{s,i}, \qquad q_{s,ij} = 0 \tag{5}$$

The diffusion exchange coefficients $D_{0,i,j}$ can be estimated according to the Vignes equation [22]:

$$D_{0,i,j} = (D_{0,i})^{\theta_i/(\theta_i+\theta_j)}(D_{0,j})^{\theta_j/(\theta_i+\theta_j)} \tag{6}$$

The following initial and boundary conditions apply:

$$t = 0, \quad 0 \leq R - r \leq \delta, \quad \theta_i = 0 \tag{7}$$

$$\begin{aligned} R - r &= 0, \quad \theta_i(R,t) = \mathrm{IAST}(P, y_i) \\ R - r &= \delta, \quad \theta_i(R-\delta, t) = 0 \end{aligned} \tag{8}$$

2.1. Solution of the proposed model

The numerical solution of the model was achieved using the method of lines (MOL) that converts partial differential equations into a system of ordinary differential equations [23]. The spatial discretization was done according to a second-order non-linear Galerkin-based method. Both the discretization and the resulting ordinary differential equations represented by matrices were solved with intrinsic codes in Matlab 6.5.1. The calculation of the matrix of thermodynamic correction factors was based on the approach of Krishna and Baur [24]. In addition to the pure compounds n-hexane (C6), n-decane (C10) and toluene (TOL), three

Table 1
Adsorption and diffusion parameters

Parameter	Hydrocarbon		
	C6	C10	TOL
$q_{i,s}$ (mol kg^{-1})	1.3	0.9	1.6
b_i ($\times 10^2$ kPa^{-1})	1.6	43.8	4.5
$D_{0,i}$ ($\times 10^{11}$ m^2 s^{-1})	8.7	2.5	0.8

different hydrocarbon mixtures were simulated, with the following C6:C10:TOL mole fractions: mixture A (0.45:0.1:0.45), mixture B (0.25:0.5:0.25) and mixture C (0.25:0.25:0.5).

The individual adsorption parameters for C6, C10 and TOL used in the simulations, b_i and $q_{i,s}$, were obtained in adsorption experiments with the pure hydrocarbons performed in a batch fluidized bed reactor [25], and diffusion parameters were taken from the literature [26]. All the parameters are shown in Table 1.

3. Results and discussion

3.1. Transient permeate fluxes

3.1.1. Permeation of the single components

The responses of the model for the case of feeding hydrocarbons individually with a step function in the outer surface of the membrane can be observed in Fig. 2. The magnitudes of the step composition changes were chosen in order to compare with the mixtures' behavior. As expected, in all the cases the permeate fluxes increase until reaching a steady value. Delays, that can be defined as the time at which the steady-state values are reached, are apparent; they are approximately 11 s for C6; about 21 s for C10 and about 56 s for TOL. It can be noticed that the faster the diffusion, the shorter the time delays. The steady-state flux for a given pure hydrocarbon can be assessed from

$$N_i = \rho_z q_{s,i} D_{0,i} \frac{\ln(1 + b_i P_{i,\text{feed}})}{R \ln(R/r)} \quad (9)$$

as derived from Eq. (2), where $P_{i,\text{feed}}$ is the partial pressure of the hydrocarbon at the feed side. This means that the flux of a pure compound depends not only on the diffusivity, but also on the equilibrium adsorption constant, the adsorption saturation capacity and the partial pressure of the species.

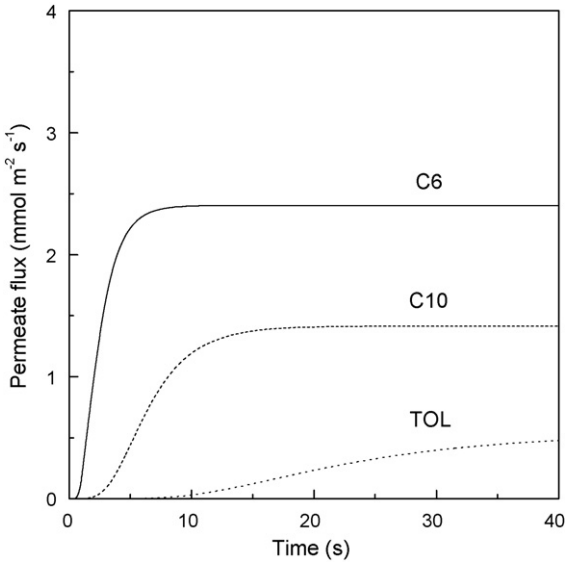

Fig. 2. Transient permeate fluxes after step changes in the concentration of the pure hydrocarbons. Feed pressure (kPa): C6 (solid line), 62.1; C10 (dashed line), 13.8; TOL (dotted line), 62.1.

3.1.2. Permeation of the mixture

Simulations were performed with ternary C6–C10–TOL mixtures. With mixture A, where the partial pressures are the same as those for the pure hydrocarbons in the example of Fig. 2, the transient permeation behavior of the components in the mixture showed that the fluxes of the hydrocarbons diffusing faster (C6 and C10) are qualitatively different from those of the single components (refer to Fig. 3a); in effect, maxima appear as a function of time before the steady-state values are reached. On the contrary, the component with slow diffusion (TOL) shows a behavior similar to that of the pure component, increasing monotonically up to the steady state. C6 diffuses very fast through the membrane, but after reaching the maximum value, its steady-state flux results lower than those of the other components, with a strong decrease from 2.40 mmol m^{-2} s^{-1} when pure to 0.72 mmol m^{-2} s^{-1} in the mixture. A similar behavior was observed for the flux of C10, changing from 1.42 mmol m^{-2} s^{-1} when pure to 0.75 mmol m^{-2} s^{-1} in the mixture. In contrast, TOL increased its steady-state flux from 0.53 mmol m^{-2} s^{-1} when pure to 1.10 mmol m^{-2} s^{-1} in the mixture. It can be observed that the time delay for C6 is significantly increased from 11 s when pure to more than 43 s in the mixture, while those of C10 and TOL remain essentially unchanged.

These observations confirm that the gradient of concentration, as assumed in the Fick formulation [27], does not constitute the actual driving force for diffusive transport in this system. Additional evidences can be observed in the simulations with mixtures B and C. The increase in the concentration of C10 in mixture B enhances its flux, moderates the peak value of the C6 flux and does not change significantly the profile of TOL, as it can be seen in Fig. 3b. It is also noticed that the maximum C6 and C10 fluxes emerge at a time slightly shorter than in the previous case. In mixture C, TOL is the component with the highest concentration; consequently its flux increases. In this case, the peak of C6 flux is moderated and C10 flux decreases in comparison with mixture B.

3.2. Transient fractional coverages

The impact of diffusion and adsorption on the transport of a hydrocarbon mixture through a Y zeolite membrane can be understood more clearly when the transient fractional coverages across the membrane are observed. These profiles are shown in Fig. 4. One of the indexes reflecting the behavior of the permeate fluxes is the slope of the fractional coverage profiles at the permeate side. In effect, in the case of mixture A, the maximum value of the slope of the C10 fractional coverage at the permeate side is achieved at approximately 10 s, which is coincident with the time at which the maximum flux is achieved (refer to Figs. 3a and 4b). Similarly, the slope of the C6 fractional coverage profile at the permeate side is maximum at approximately 5 s, in coincidence with the peak value in C6 flux (refer to Figs. 3a and 4a). Note that at certain time and position in the membrane, the fractional coverages of both C6 and C10 overshoot the steady-state values. TOL achieves its maximum slope for its fractional coverage at the permeate side at the steady state, thus indicating maximum flux at that moment (refer to Figs. 3a and 4c).

The characteristics of the adsorption of the mixture influence the fluxes of the species by setting the magnitudes of the driving forces $\nabla\theta_i$ and by contributing to the coupling of the diffusion and adsorption processes shown in the non-diagonal elements in the matrices of the thermodynamical correction factors $\boldsymbol{\Gamma}$ and sorbate–sorbate interactions $\mathbf{B}$, as shown in Eq. (2).

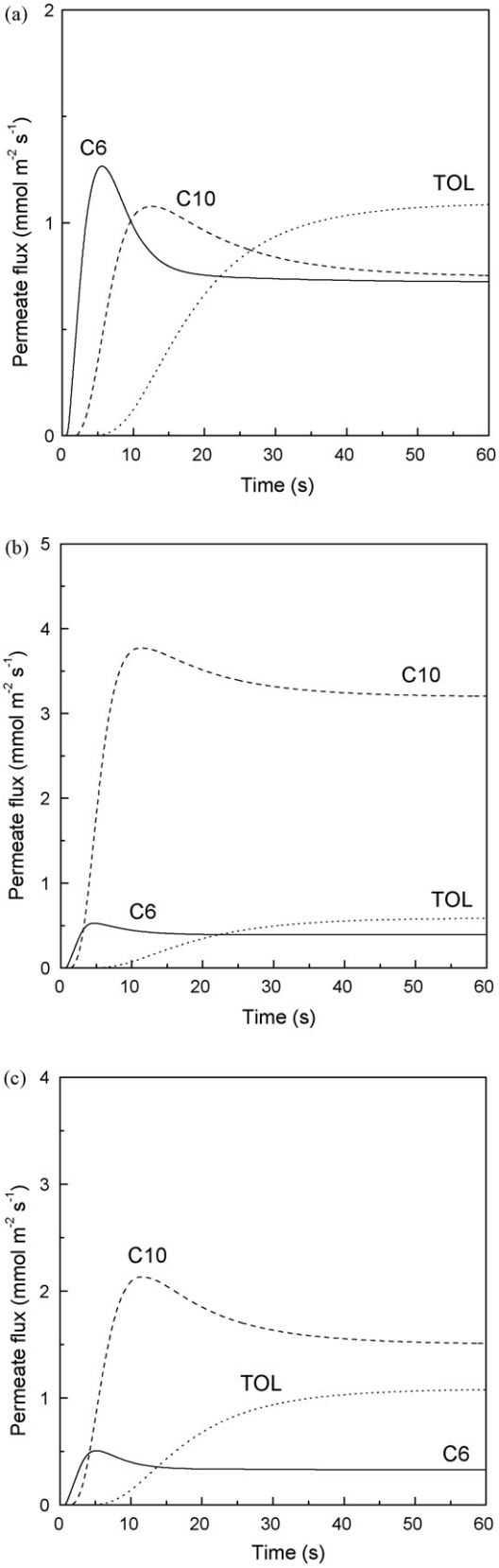

Fig. 3. Transient permeate fluxes after step changes in concentration. Ternary mixture of hydrocarbons. Feed pressure: 137.9 kPa. (a) Mixture A; (b) mixture B; (c) mixture C.

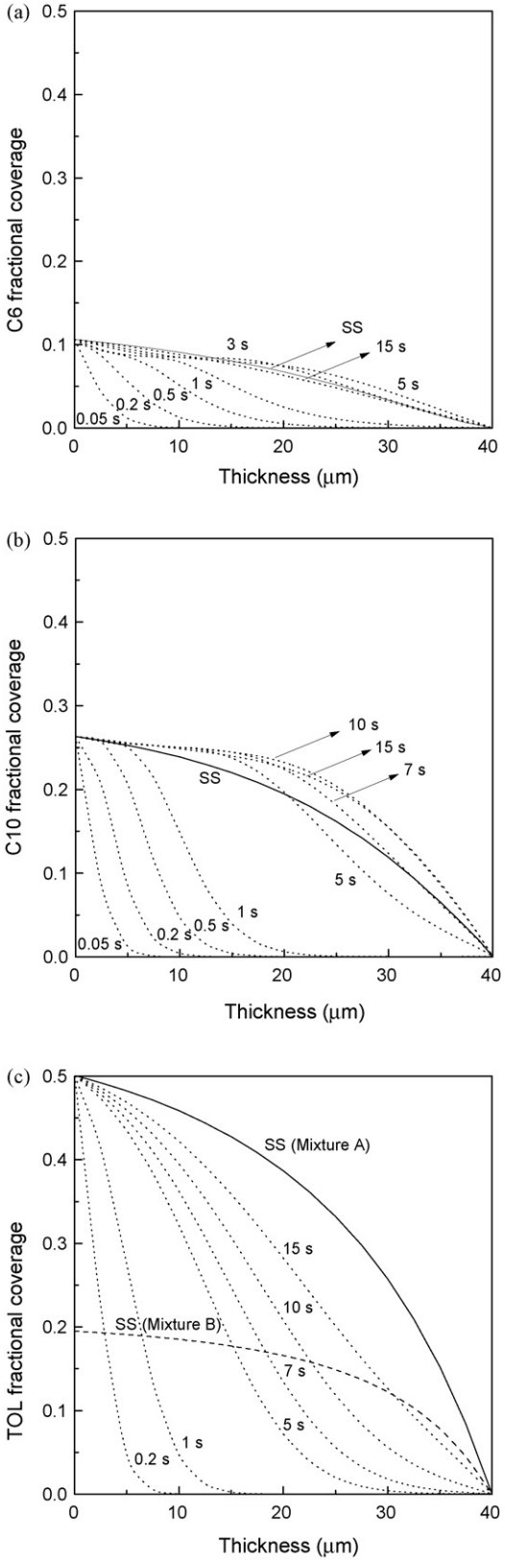

Fig. 4. Transient fractional coverages across the membrane in the case of mixture A. Feed pressure: 137.9 kPa. (a) C6; (b) C10; (c) TOL.

Table 2
Fractional coverages on the feed side of the membrane for the ternary mixtures

Mole composition (C6:C10:TOL)	C6	C10	TOL
(A) 0.45:0.10:0.45	0.106	0.264	0.500
(B) 0.25:0.50:0.25	0.038	0.722	0.193
(C) 0.25:0.25:0.50	0.044	0.439	0.433

Feed pressure: 137.9 kPa.

The same correspondence between the spatial rates of change of the fractional coverages at the permeate side of the membrane and fluxes can be observed at the steady states, as can be confirmed particularly in Fig. 4c for the case of TOL in mixtures A and B; in effect, at the steady state, the higher the slope at the permeate side, the higher the flux. However, as it can be inferred from Fig. 4c, the slope at the permeate side depends on how much the hydrocarbon is adsorbed at the feed side. Therefore, the coverage (or concentration) of each adsorbate at the feed side, according to the mixture adsorption isotherm, and the diffusivity, are the properties controlling the magnitudes of the steady-state fluxes across the membrane. Hence, depending on which effect prevails, i.e., magnitudes of adsorption or diffusivities, will determine the permeation behavior of the mixture.

Table 2 shows the fractional coverages of the species on the feed side of the membrane, which are equivalent to equilibrium adsorbate concentrations, for the various mixture compositions. In the case of mixture A, TOL coverage on the feed side is high enough to overcome its slower diffusion, thus leading to the highest flux. In this case, the much higher adsorption strength of C10 does not compensate its low concentration in the gas phase and its lower packing entropy according to the larger molecular size. However, in the case of mixture B, C10 adsorbate concentration on the feed side is larger than those of the other hydrocarbons; considering that $D_{0,C10}$ is significant, both effects contribute positively to make its permeate flux the highest in the mixture. In the case of mixture C, despite the fact that TOL achieves a coverage on the feed side similar to that of C10, it is not enough to compensate for its slow diffusion, and hence, C10 permeate flux is larger. Moreover, even though C6 has the highest diffusivity in the group, its permeate flux is always the lowest, mainly due to its low surface coverage in the mixture equilibria on the feed side as a consequence of its weaker adsorption strength.

3.3. Permeances and permeance selectivities

3.3.1. The effect of pressure

Permeances (pressure normalized fluxes) are also used to characterize gas transport through membranes; they are defined as

$$\Pi_i = \frac{N_i}{\Delta P_i} \tag{10}$$

where ΔP_i is the partial pressure drop across the membrane of the permeating component. The permeances of the diverse hydrocarbons obtained at the steady state can be observed in Fig. 5 as a function of pressure for the case of an equimolar ternary mixture, that is, with the same ΔP_i. It can be seen that the various permeances decrease with similar trends as pressure increases, the ranking being C10 > TOL > C6 in the whole range of pressures used, except at very low pressures. The simulations assuming linear isotherms for all the components lead to constant permeances. This predicted behavior of the permeances is consistent with the shapes of the equilibrium isotherms; van den Broeke et al. [28] showed that the permeances have non-linear dependences on pressure when the isotherms are of the Langmuir type, while linear isotherms would show almost constant permeances.

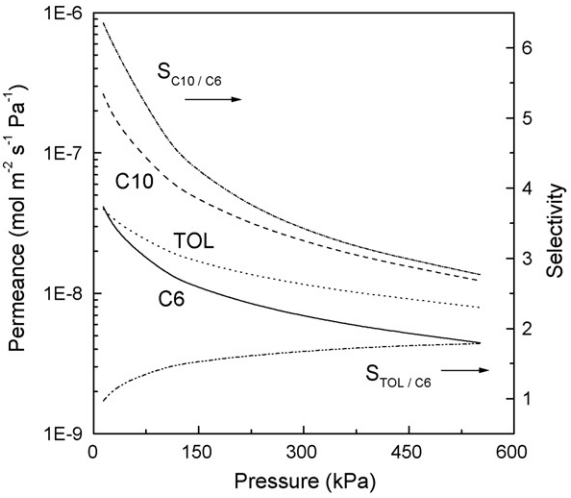

Fig. 5. Permeance and permeance selectivities as a function of pressure. Equimolar ternary mixture. C6: solid line; C10: dashed line; TOL: dotted line. Selectivities: C10/C6 (short dash dot line); TOL/C6 (dash dot dot line).

The experimental information about permeances in similar mixtures is scarce, thus making difficult to establish comparisons. For instance, Jeong et al. [29] reported permeances of hexane in binary mixtures with dimethylbutane or methylpentane over 5–10 μm NaY zeolite membranes to be about 1×10^{-8} mol m^{-2} s^{-1} Pa^{-1} at 100–140 °C and 4.5 kPa total pressure. In the equimolar ternary mixture simulated in this work, for example, the permeance of C6 at 250 °C and 13.8 kPa total pressure would be about 4.2×10^{-8} mol m^{-2} s^{-1} Pa^{-1}. In this case, the positive effect of the higher temperature should be somewhat offset by the longer path across the membrane.

From the technology point of view, it may be more interesting to learn about the feasibility of separation or concentration of a hydrocarbon mixture through given membranes and conditions. The model allows to predict the permeance selectivities, defined as the ratios between permeances, if a hydrocarbon is defined as a reference, C6 in this case. The simulation results are included in Fig. 5, and they indicate that C10 selectivity is important and increases dramatically at lower pressures. TOL selectivity is relatively low and increases with the system pressure; at low pressure it may be lower than one, because C6 and TOL isotherms come close to linear and the permeation fluxes are dependent only on diffusivities and Henry constants. In effect, it can be seen from Van De Graaf et al. [30] that the selectivity at diluted conditions can be evaluated as

$$S_{i,j} = \frac{D_{0,i}K_i}{D_{0,j}K_j} \tag{11}$$

and according to the corresponding diffusion and adsorption parameters, this ratio is lower than one.

The behavior of the selectivities is linked to the relationship between the mixture isotherm and the system pressure. For the equimolar mixture, there is a significant increase in TOL coverage with pressure at the feed side, while C10 coverage decreases after reaching a maximum value (see Fig. 6). Thus, as pressure increases, the entropic control of adsorption [31], that favors the packing of TOL molecules as compared to C10, becomes more pronounced, thus enhancing its adsorption selectivity in relation to the other hydrocarbons.

3.3.2. The effect of mixture composition

To analyze the effect of the composition of the mixtures in terms of the changes in the permeances, their selectivities, and the

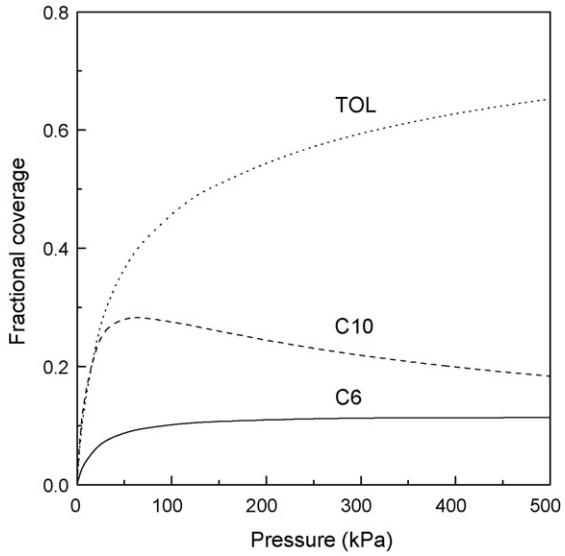

Fig. 6. Fractional coverage at the feed side of the membrane as a function of pressure according to IAST isotherm. Equimolar ternary mixture. Temperature: 250 °C.

equilibrium adsorption selectivities, a feed pressure of 137.9 kPa was considered, keeping C6 as the reference hydrocarbon. It can be seen in Fig. 7 that the permeance of TOL decreases slightly with the increase of its mole fraction in the gas phase, approaching to the value of pure TOL. The permeance of C10 also decreases slightly, while that of the reference hydrocarbon, C6, decreases more noticeably.

As a consequence, both TOL and C10 permeance selectivities increase with larger TOL mole fractions, even though the equilibrium adsorption selectivities at the feed side, calculated with the IAST isotherm:

$$S_{i,j}^{eq} = \frac{q_i^{eq}/P_i}{q_j^{eq}/P_j} \quad (12)$$

remain essentially constant, as shown in Table 3. These results indicate that the transport rate of C6 across the membrane is hindered by the increasing fractional coverage of TOL, as is reflected in the increasing sorbate–sorbate interaction shown by the variation in the corresponding diffusion exchange coefficients $D_{0,C6,TOL}$,

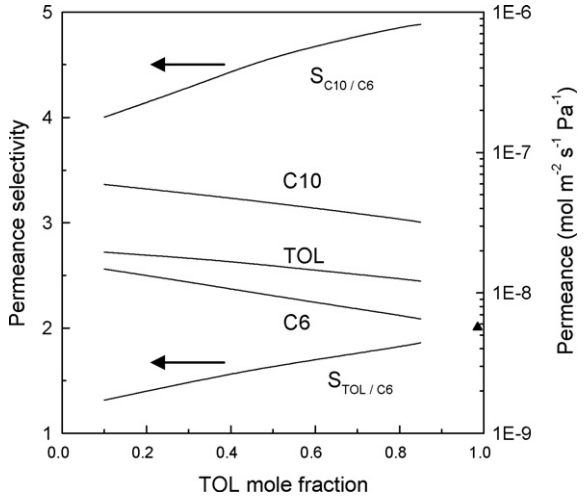

Fig. 7. Permeance and permeance selectivities as a function of TOL concentration. Feed pressure: 137.9 kPa. (▲) Pure TOL permeance.

Table 3
Diffusion exchange coefficients and equilibrium adsorption selectivities at the feed side as a function of mixture composition, starting from equimolar mixture

	$D_{0,i,j}$ ($\times 10^{11}$ cm^2/s)			$S^{eq}_{C10,C6}$	$S^{eq}_{TOL,C6}$
	$D_{0,C6,C10}$	$D_{0,C6,TOL}$	$D_{0,C10,TOL}$		
y_{TOL}					
0.33	2.80	1.19	1.71	7.20	6.14
0.50	2.80	0.99	1.42	7.23	6.13
0.90	2.79	0.82	0.90	7.35	6.08
y_{C10}					
0.33	2.80	1.19	1.71	7.20	6.14
0.50	2.66	1.18	1.97	6.83	6.29
0.90	2.52	1.17	2.41	6.26	6.55

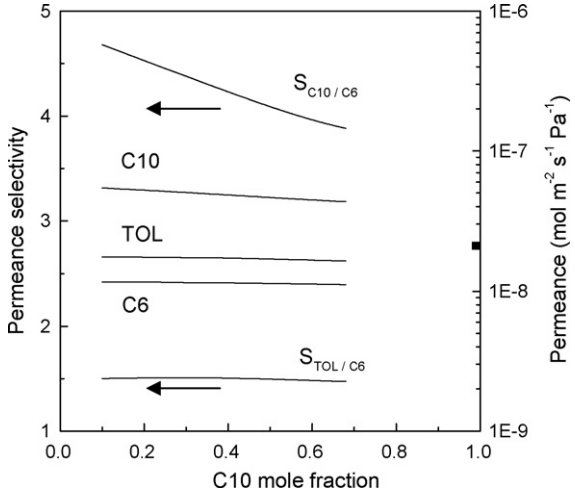

Fig. 8. Permeance and permeance selectivities as a function of C10 concentration. Feed pressure: 137.9 kPa. (■) Pure C10 permeance.

approaching the diffusivity of pure TOL, 0.8×10^{-11} cm^2/s (refer to Table 3). Indeed, the transport rate of C10 is also affected, but the corresponding diffusion exchange coefficients $D_{0,C10,TOL}$ are more distant from TOL diffusivity than those of C6, thus reflecting a lower interaction.

The changes in the permeances induced by higher concentrations of C10 in the mixture are smoother, as shown in Fig. 8. The permeance of C10 decreases to its value when pure, while those of TOL and C6 remain almost steady. As a consequence, the permeance selectivity of C10 decreases and that of TOL is constant with larger C10 mole fractions. The decrease in C10 permeance selectivity is consistent with the trend in its equilibrium adsorption selectivity (refer to Table 3). However, the hindering effect of C10 is lower than the one observed with TOL, as shown by the smaller changes in the interaction between diffusing species, indicated by the diffusion exchange coefficients $D_{0,i,j}$ in Table 3.

The equilibrium adsorption selectivity of TOL in the mixture, i.e., $S^{eq}_{TOL,C6}$, increases slightly with higher C10 concentrations and the exchange coefficient $D_{0,C6,TOL}$ is not appreciably modified. Consequently, the equilibrium adsorption and diffusion effects seem to compensate each other, resulting in a constant permeance selectivity as C10 coverage increases.

4. Conclusions

The modelling and simulation of the permeation of a ternary mixture of hydrocarbons through a Y zeolite cylindrical membrane, based on the Maxwell–Stefan formulation and the IAST isotherm, allow to predict the transient permeate fluxes of the mixture

components. As a consequence of the interactions between the hydrocarbons in the mixture strong variations in the fluxes arise in comparison to the fluxes when the species are fed pure. Moreover, the fluxes of the species diffusing faster (C6 and C10) overshoot the steady-state values. The magnitudes of the fluxes depend on the surface coverage profiles across the membrane, the sorbate–sorbate interactions and the adsorption equilibrium at the feed side. The permeances have the same order of magnitude as those scarcely reported in the literature.

The prediction of the permeance selectivities in the mixture shows variations with feed pressure and composition. These results suggest that the operative conditions can bring about modifications in the separation performance of the zeolite membrane on a mixture composed of species with different diffusion and adsorption properties.

According to this model, the feasibility of separation of different mixtures by means of a zeolite membrane process can be studied.

Acknowledgements

This work was performed with the financial assistance of Universidad Nacional del Litoral, Secretaría de Ciencia y Técnica (Santa Fe, Argentina) Proj. 01-07, Consejo Nacional de Investigaciones Científicas y Técnicas (CONICET) PIP 6285/05, and Agencia Nacional para la Promoción Científica y Tecnológica PICT05 14-32930.

References

[1] Y.S. Wan, J.L.H. Chau, A. Gavriilidis, K.L. Yeung, Design and fabrication of zeolite-based microreactors and membrane microseparators, Microporous Mesoporous Mater. 42 (2001) 157–175.
[2] L. Kiwi-Minsker, A. Renken, Microstructured reactors for catalytic reactions, Catal. Today 110 (2005) 2–14.
[3] A. Zampieri, P. Colombo, G.T.P. Mabande, T. Selvam, W. Schwieger, F. Scheffler, Zeolite coatings on microcellular ceramic foams: a novel route to microreactor and microseparator devices, Adv. Mater. 16 (2004) 819–823.
[4] M. Vilaseca, J. Coronas, A. Cirera, A. Cornet, J.R. Morante, J. Santamaría, Use of zeolite films to improve the selectivity of reactive gas sensors, Catal. Today 82 (2003) 179–185.
[5] J. de Jong, R.G.H. Lammertink, M. Wessling, Membranes and microfluidics: a review, Lab Chip 6 (2006) 1125–1139.
[6] J. Coronas, J. Santamaría, The use of zeolite films in small-scale and micro-scale applications, Chem. Eng. Sci. 59 (2004) 4879–4885.
[7] L. Van Den Broeke, W. Bakker, F. Kapteijn, J. Moulijn, Binary permeation through a silicalite-1 membrane, AIChE J. 45 (1999) 976–985.
[8] E.E. McLeary, J.C. Jansen, F. Kapteijn, Zeolite based films, membranes and membrane reactors: progress and prospects, Microporous Mesoporous Mater. 90 (2006) 198–220.
[9] R. Krishna, R. Baur, Modelling issues in zeolite based separation processes, Sep. Purif. Technol. 33 (2003) 213.
[10] A.L. Myers, J.M. Prausnitz, Thermodynamics of mixed-gas adsorption, AIChE J. 11 (1965) 121–127.
[11] F. Kapteijn, J.A. Moulijn, R. Krishna, The generalized Maxwell–Stefan model for diffusion in zeolites: sorbate molecules with different saturation loadings, Chem. Eng. Sci. 55 (2000) 2923–2930.
[12] A. Salem, A.A. Ghoreyshi, M.A. Jahanshahi, Multicomponent transport model for dehydration of organic vapors by zeolite membranes, Desalination 193 (2006) 35–42.
[13] J.G. Martinek, T.Q. Gardner, R.D. Noble, J.L. Falconer, Modeling transient permeation of binary mixtures through zeolite membranes, Ind. Eng. Chem. Res. 45 (2006) 6032–6043.
[14] H. Qinglin, S. Farooq, I.A. Karimi, Binary and ternary adsorption kinetics of gases in carbon molecular sieves, Langmuir 19 (2003) 5722–5734.
[15] A.M. Avila, C.M. Bidabehere, U. Sedran, Assessment and modeling of adsorption selectivities in the transport of mixtures of hydrocarbons in FCC catalyst, Ind. Eng. Chem. Res. 47 (2007) 7927–7935.
[16] S.K. Wirawan, D. Creaser, Multicomponent $H_2/CO/CO_2$ adsorption on BaZSM-5 zeolite, Sep. Purif. Technol. 52 (2006) 224–231.
[17] Breck Zeolite Molecular Sieves: Structure, Chemistry, and Use, John Wiley & Sons, New York, 1974.
[18] Y. Hasegawa, K. Watanabe, K. Kusakabe, S. Morooka, Influence of alkali cations on permeation properties of Y-type zeolite membranes, J. Membr. Sci. 208 (2002) 415–418.
[19] K. Kusakabe, T. Kuroda, A. Murata, S. Morooka, Formation of a Y-type zeolite membrane on a porous alpha-alumina tube for gas separation, Ind. Eng. Chem. Res. 36 (1997) 649–655.
[20] Gu, et al., Synthesis of defect-free FAU-type zeolite membranes and separation for dry and moist CO_2/N_2 mixtures, Ind. Eng. Chem. Res. 44 (2005) 937–944.
[21] K. Weh, M. Noack, I. Sieber, J. Caro, Permeation of single gases and gas mixtures through faujasite-type molecular sieve membranes, Microporous Mesoporous Mater. 54 (2002) 27–36.
[22] A. Vignes, Diffusion in binary solutions, Ind. Eng. Chem. Fundam. 5 (1966) 189–199.
[23] S.C. van der Linde, T.A. Nijhuis, F.H.M. Dekker, F. Kapteijn, J.A. Moulijn, Mathematical treatment of transient kinetic data: combination of parameter estimation with solving the related partial differential equations, Appl. Catal. A: Gen. 151 (1997) 27.
[24] R. Krishna, R. Baur, Diffusion, adsorption and reaction in zeolites: modelling and numerical issues, http://ct-cr4.chem.uva.nl/zeolite/, November 10, 2003.
[25] A.M. Avila, C.M. Bidabehere, U. Sedran, Diffusion and adsorption selectivities of hydrocarbons over FCC catalysts, Chem. Eng. J. 132 (2007) 67.
[26] J. Karger, D. Ruthven, Diffusion in Zeolites and Other Microporous Solids, John Wiley & Sons, NY, 1992.
[27] D.M. Ruthven, Sorption kinetics for diffusion-controlled systems with a strongly concentration-dependent diffusivity, Chem. Eng. Sci. 59 (2004) 4531.
[28] L.J.P. van den Broeke, W.J.W. Bakker, F. Kapteijn, J.A. Moulijn, Transport and separation properties of a silicalite-1 membrane. Operating conditions, Chem. Eng. Sci. 54 (1999) 245–258.
[29] B. Jeong, Y. Hasegawa, K. Sotowa, K. Kusakabe, S. Morooka, Vapor permeation properties of an NaY-type zeolite membrane for normal and branched hexanes, Ind. Eng. Chem. Res. 41 (2002) 1768–1773.
[30] J.M. Van De Graaf, F. Kapteijn, J.A. Moulijn, Modeling permeation of binary mixtures through zeolite membranes, AIChE J. 45 (3) (1999) 497–511.
[31] R. Krishna, S. Calero, B. Smit, Investigation of entropy effects during sorption of mixtures of alkanes in MFI zeolite, Chem. Eng. J. 88 (2002) 81.